J. Plasma Phys. (2018), *vol.* 84, 905840202 © Cambridge University Press 2018
doi:10.1017/S0022377818000223

Twisted waves and instabilities in a permeating dusty plasma

S. Bukhari[1,2,†], S. Ali[1,2,3], S. A. Khan[2] and J. T. Mendonca[4]

[1]Department of Physics, The University of Azad Jummu and Kashmir, Muzaffarabad 13100, Azad Kashmir

[2]National Center for Physics at Quaid-e-Azam University Campus, Shahdra Valley Road, Islamabad 44000, Pakistan

[3]Hefei National Laboratory for Physical Sciences at Microscale and Department of Physics, University of Science and Technology of China, 96 Jinzhai Road, Hefei, Anhui 230026, PR China

[4]IPFN, Instituto Superior Tecnico, Av. Rovisco Pais 1, 1049-001 Lisboa, Portugal

(Received 23 October 2017; revised 19 February 2018; accepted 19 February 2018)

New features of the twisted dusty plasma modes and associated instabilities are investigated in permeating plasmas. Using the Vlasov–Poisson model equations, a generalized dispersion relation is obtained for a Maxwellian distributed plasma to analyse the dust-acoustic and dust-ion-acoustic waves with finite orbital angular momentum (OAM) states. Existence conditions for damping/growth rates are discussed and showed significant modifications in twisted dusty modes as compared to straight propagating dusty modes. Numerically, the instability growth rate, which depends on particle streaming and twist effects in the wave potential, is significantly modified due to the Laguerre–Gaussian profiles. Relevance of the study to wave excitations due to penetration of solar wind into cometary clouds or interstellar dusty plasmas is discussed.

Key words: astrophysical plasmas, dusty plasmas, plasma instabilities

1. Introduction

The observations by the Cassini radio and plasma wave science instruments have exclusively confirmed (Yaroshenko *et al.* 2009) the existence of negatively charged dust grains in Enceladus's orbit that caused a depletion of electrons in the background plasma. In 2011, particle-in-cell (PIC) simulations (Yaroshenko *et al.* 2011) were carried out to examine the strong dependence of plasma density perturbations and potential profile around the orbiter on the energy distribution during the interaction of Saturn's magnetosphere with a spherical orbiter via the Saturn orbit insertion flyby trajectory. The dust charging mechanism (Yaroshenko, Luhr & Miloch 2014) was also discussed by utilizing the Cassini data to observe the reduction of electrical potential and dust charging time in dust-diluted regions of the Enceladus plasma environment. Later, PIC simulations (Yaroshenko, Miloch & Lühr 2015) were performed to investigate the Cassini spacecraft interaction with co-rotating

† Email address for correspondence: shujaht_physics@yahoo.com

https://doi.org/10.1017/S0022377818000223 Published online by Cambridge University Press

plasma flowing in the Enceladus torus and examined the presence of dust grains. Klumov, Vladimirov & Morfill (2005) have focused on the dust grain composition and associated optical properties for dust layer formation in the mesosphere. It was shown that the interaction of solar radiation with dust grains results in dust heating and photoelectron emission and dust grains in the upper atmosphere reduce the concentration of water vapours significantly. The authors (Klumov, Vladimirov & Morfill 2007) also used a kinetic description to study the impact of dust grains on the composition of the plasma in cometary comae.

The heating of a cometary nucleus as it approaches the Sun is responsible for its large atmosphere and associated dust and plasma environment (Mendis & Horanyi 2013). The atmosphere is typically 10^4–10^6 times larger than the dimension of the nucleus. Cometary dusty plasma environments have been recognized as natural space laboratories for studying dust–plasma interactions, wave dynamics and its physical consequences as confirmed by International Cometary Explorer (ICE) spacecraft fly-by through the tail of comet Giacobini–Zinner in 1985 and the Vega 1 and 2, and Giotto spacecraft fly-bys of comet Halley in 1986 (Mendis 1988; Festau, Keller & Weaver 2004). In the course of the passage of the comet Halley, there was a clear observation of the waves and oscillations occurring in cometary plasmas with frequencies as low as 10 Hz (Grard *et al.* 1986; Klimov *et al.* 1986). The composition of such cometary plasmas depends on their distance from the coma. It is believed that the predominant constituents include charged grains and various ions of hydrogen, carbon, water, oxygen, sodium, etc. with pick-up ions of H from the solar wind plasma (Balsiger *et al.* 1986). Similar observations of a coma have been revealed by the Rosetta spacecraft of the European Space Agency (ESA) orbiting close to comet 67P/Churyumov Gerasimenko through its ROSINA experiment (Wurz *et al.* 2015). The solar wind plasma in the atmosphere penetrates the cometary cloud which increases the complexity of the system. The whole system becomes potentially unstable due to the availability of free energy stored in the solar wind species streaming through the coma.

Normally, the constituents of the solar wind plasma are electrons and protons, while a cometary plasma is a multi-component plasma including electrons, positive ions and dust particulates. The streaming solar wind plasma behaves as a source of free energy which ultimately excites the dust-acoustic (DA) wave on dust time scales. In the presence of an electron drift relative to ions, the existence of an ion-acoustic wave with a kinetic instability was identified by (Vranjes & Poedts 2014). Some unique features of the kinetic instability were pointed out by the authors. Vranjes (2011) carried out a theoretical investigation of DA instability in cometary tails due to solar wind interaction and examined a threshold limit for instability. Gong, Liu & Du (2012*a*) studied the DA instability in a permeating dusty plasma with a Maxwellian distribution of plasma constituents. The authors presented the unstable modes due to flowing velocity for the case when the solar wind thermal velocity is much greater than the phase velocity of the DA wave, whereas in the reverse case the instability appears only at smaller wavenumber with large flowing velocity. The authors further extended their idea for studying DA wave instability with a power-law distribution by incorporating non-extensive q-statistics (Gong, Liu & Du 2012*b*). It has been shown that non-extensive effects play a significant role in defining the stability of the DA wave in the limit of small wavenumbers.

The existence of a co-rotating solar wind and angular momentum attributed to the plasma particles have been identified by the investigations (Grewing, Praderie & Reinhard 1988) of comet Halley. If the rotating solar wind interacts with a cometary

https://doi.org/10.1017/S0022377818000223 Published online by Cambridge University Press

plasma, then plasma particles experience an angular momentum. Many situations in the solar corona and solar wind show the existence of helical field structures, for example, in coronal plasmas, in interplanetary clouds, in solar jets, etc. The formation of vortices (Sibeck 1990) can result due to the interaction of solar wind pressure pulses with the Earth's magnetosphere. The angular momentum from a moving plasma vortex structure can be transferred due to spinning motions which leads to anomalous behaviour of waves and structures in the solar wind (Lundin & Marklund 1995). The existence of helical phase surfaces has been recognized in space plasmas showing a strong impact of the angular momentum on the wave propagation of helicons (Stenzel 2016).

In recent years, a great deal of interest has been noticed in studying twisted waves with finite orbital angular momentum (OAM) in plasmas (Mendonca, Thide & Then 2009; Mendonca 2012; Shukla 2012; Khan, Rehman & Mendonca 2014; Shahzad & Ali 2014; Ali, Bukhari & Mendonca 2016; Bukhari *et al.* 2017). It was shown that pumping a plasma with radiation beams carrying finite OAM states produces stimulated Raman and stimulated Brillouin scattering which give rise to plasma waves themselves carrying OAM (Mendonca *et al.* 2009). Mendonca (2012) also identified twisted electron plasma waves with finite OAM in the kinetic theoretical framework. The idea of the OAM states in plasma waves was extended by using the Laguerre Gaussian (LG) beam solutions to kinetically investigate the twisted ion-acoustic (IA) plasma vortices (Khan *et al.* 2014) and twisted electron-acoustic (EA) waves in the hydrodynamic regime (Shahzad & Ali 2014). Investigations of twisted plasma waves continued in multi-component plasmas as well. Recently, Ali *et al.* (2016) studied twisted waves in multi-component dusty plasmas, deriving the modified dispersion relations for DA and dust-ion-acoustic waves using the Maxwellian distribution of particles. The influence of the twist parameter and dust concentration on the Landau damping rate was emphasized. The instability of twisted waves in the kappa distributed multi-component dusty plasma was also investigated by Arshad *et al.* (2017), to studying the dependence of the growth rate on various plasma parameters.

In the present work, kinetic instabilities due to twisted dust-acoustic (DA) and dust-ion-acoustic (DIA) waves are investigated and the influence of OAM states is examined when the solar (stellar) wind propagates through an interplanetary (interstellar) plasma. The solar wind plasma usually contains electron and ion species, while interplanetary plasma consists of electrons, ions and dust particles. For the investigation of wave dynamics, a Vlasov–Poisson kinetic model is used for an unmagnetized permeating plasma with a Maxwellian distribution. A generalized expression for the plasma dielectric constant is derived to study the dispersion properties and instability thresholds of DA and DIA waves.

The paper is organized as follows: In § 2, the model equations and basic assumptions for the twisted dust-acoustic and dust-ion-acoustic waves are considered for a permeating Maxwellian plasma. In §§ 3 and 4, the twisted wave frequency and instability growth rate of the twisted DA and DIA waves carrying finite OAM states are analysed, respectively. The numerical description of the wave instabilities along with a summary of the work are presented in § 5.

2. Dielectric constant with finite OAM states

Let us consider a fast flowing solar wind (electrons and ions) plasma penetrating through a relatively slow moving plasma containing electrons, singly ionized positive ions $Q_i(= Z_i e)$ and negatively charged dust grains $Q_d(= -Z_d e)$ where $Q_i(Q_d)$

https://doi.org/10.1017/S0022377818000223 Published online by Cambridge University Press

represents the charge of ions (dust grains), 'e' being the electronic charge and $Z_i(Z_d)$ is the charge state of ions (dust grains), respectively. On a global scale, the permeating plasma holds the equilibrium charge-neutrality condition, as $\sum_j Q_j n_{j0} = 0$, where $j = f_{e,i}$ for fast electrons and ions while $j = s_{e,i,d}$ for slow moving electrons, ions and dust grains with n_{j0} the equilibrium number densities of the fast and slow moving species. The charge on the surface of dust particulates is assumed to be constant by assuming the dust charging time is much smaller than the dust plasma period. Upon perturbation from the equilibrium state, the plasma distribution function and number densities can be expressed as; $f_j = f_{j0} + f_{j1}$ and $n_j = n_{j0} + n_{j1}$. The subscripts 0 and 1 represent the equilibrium and perturbed states, respectively. The external electric and magnetic fields ($\boldsymbol{E}_0$, $\boldsymbol{B}_0$) are assumed to be zero so that a field free plasma is under consideration. The dynamical behaviour of such a plasma can be described by considering the linearized set of Vlasov–Poisson coupled equations:

$$(\partial_t + \boldsymbol{v}_j \cdot \nabla) f_{j1}(\boldsymbol{r}, \boldsymbol{v}_j, t) - \frac{Q_j}{m_j} \nabla \phi_1 \cdot \nabla_{\boldsymbol{v}_j} f_{j0}(\boldsymbol{v}_j) = 0, \tag{2.1}$$

and

$$\nabla^2 \phi_1 = -\sum_j 4\pi Q_j \int f_{j1}(\boldsymbol{r}, \boldsymbol{v}_j, t)\, \mathrm{d}\boldsymbol{v}_j. \tag{2.2}$$

Here $f_{j0}(\boldsymbol{v}_j)$ represents the Maxwellian distribution function, ∇ is the usual three-dimensional space operator and $\nabla_{\boldsymbol{v}_j}$ is an operator in the velocity coordinate system.

For twisted electrostatic waves, we make use of the LG profiles for perturbed quantities such as the distribution function f_{j1} and the electrostatic potential ϕ_1 and their dependence on $\exp[\mathrm{i}(l\varphi + kz - \omega t)]$, where $l(= 0, \pm 1, \pm 2 \ldots)$ is the azimuthal mode index proportional to the OAM along the z-direction and φ is the azimuthal angle representing the helical phase structure. The mathematical forms and detailed explanation of these perturbed quantities are expressed in Mendonca (2012) and Ali *et al.* (2016). Thus, following the standard procedures (Mendonca 2012 and Ali *et al.* 2016), we finally obtain a kinetic dispersion relation in this form

$$D(k, \acute{k}, \omega) = 1 + \sum_j \frac{1}{k^2 \lambda_{Dj}^2} [2 + C_{zj} Z(C_{zj}) + C_{\varphi j} Z(C_{\varphi j})], \tag{2.3}$$

where $Z(C_{zj})$ and $Z(C_{\varphi j})$ are the well-known axial and azimuthal plasma dispersion functions, $\lambda_{Dj}[= T_j/4\pi n_{j0} e^2]$ is the Debye length of the jth species. The arguments for the fast and slow moving plasma species can be defined, as $C_{z,fe,i} = (u_z - k v_{f0})/v_{t,fe,i}$, $C_{z,se,si,sd} = u_z/v_{t,se,si,sd}$ and $C_{\varphi j} = u_\varphi/v_{tj}$. Here $v_{f0}[= v_{fe0} = v_{fi0}]$ is the streaming velocity of fast moving species, $u_z = (\omega - \acute{k} v_\varphi)/k$ and $u_\varphi = (\omega - k v_z)/\acute{k}$, $\acute{k}(= l q_\varphi)$ and k are the azimuthal and longitudinal wavenumbers, respectively. Equation (2.3) is the generalized dispersion relation (*viz.*, $D(k, \acute{k}, \omega) = 0$) with a twist in the wave propagation.

3. Twisted DA waves and instability

First, to examine the twist effect on the properties of low-frequency DA waves in a permeating plasma, we impose the inequalities $v_{tsd} \ll v_{ph} \ll v_{t,se}, v_{t,si}$ on the phase speed ($v_{ph} = \omega/k$) of the waves, where $v_{t,sd}$, $v_{t,si}$, $v_{t,se}$ and $v_{t,fe}$ are the thermal speeds due to dust grains, slow moving ions and electrons and fast flowing electrons, respectively. Thus, we analyse the dispersion relation (3) for two limiting cases.

https://doi.org/10.1017/S0022377818000223 Published online by Cambridge University Press

3.1. *Low phase speed*

In the low phase speed limit $v_{ph} - v_{f0} \ll v_{t,fi}$, we consider the small argument expansions for fast moving electrons and ions as well as slow moving electrons and ions, *viz.*, $C_{z,fe}$, $C_{z,fi}$, $C_{z,se}$, $C_{z,si} \ll 1$, whereas the large argument expansion is assumed for inertial dust grains, *viz.*, $C_{z,sd} \gg 1$. The azimuthal part is considered for a large argument expansion, as $C_{\varphi j} \gg 1$. Employing the expansions and performing straightforward mathematical steps, (2.3) can be expressed (Gong *et al.* 2012*a*) for OAM states, as

$$\begin{aligned} D(k,\acute{k},\omega) \;=\; & 1+\frac{1}{k^2\lambda_{Deff}^2}-\frac{\omega_{p,sd}^2}{\omega^2}\left(1+\frac{1}{\eta^2}\right)-\frac{3k^2v_{t,sd}^2\omega_{p,sd}^2}{2\omega^4}\left(1+\frac{1}{\eta^4}\right) \\ & +2i\sqrt{\pi}\left[\frac{\omega\omega_{p,se}^2}{k^3v_{t,se}^3}\times\left\{1+\eta\exp\left(-\eta^2\frac{\omega^2}{k^2v_{t,se}^2}\right)\right\}+\frac{\omega\omega_{p,si}^2}{k^3v_{t,si}^3}\right. \\ & \times\left\{1+\eta\exp\left(-\eta^2\frac{\omega^2}{k^2v_{t,si}^2}\right)\right\}+\frac{\omega\omega_{p,sd}^2}{k^3v_{t,sd}^3}\left\{\exp\left(-\frac{\omega^2}{k^2v_{t,sd}^2}\right)\right. \\ & \left.+\eta\exp\left(-\eta^2\frac{\omega^2}{k^2v_{t,sd}^2}\right)\right\}+\left(\omega-kv_{f0}\right)\left\{\frac{\omega_{p,fe}^2}{k^3v_{t,fe}^3}+\frac{\omega_{p,fi}^2}{k^3v_{t,fi}^3}\right\} \\ & \left.+\frac{\omega\omega_{p,fe}^2}{k^3v_{t,fe}^3}\eta\exp\left(-\eta^2\frac{\omega^2}{k^2v_{t,fe}^2}\right)+\frac{\omega\omega_{p,fi}^2}{k^3v_{t,fi}^3}\eta\exp\left(-\eta^2\frac{\omega^2}{k^2v_{t,fi}^2}\right)\right], \end{aligned} \tag{3.1}$$

where $\lambda_{Deff}[=(\lambda_{Dse}^{-2}+\lambda_{Dsi}^{-2}+\lambda_{Dfe}^{-2}+\lambda_{Dfi}^{-2})^{-1/2}]$ is the effective Debye length due to slow and fast moving electrons and ions and the parameter $\eta(=k/\acute{k})$ is the ratio of plane wavenumber (k) to the azimuthal wavenumber (lq_{φ}) owing to helical phase structure of the electric field. The real part of the dielectric constant ($D_r = 0$) gives the electrostatic DA wave frequency (Gong *et al.* 2012*a*) with finite OAM, as

$$\omega_r = k\lambda_{Deff}\omega_{p,sd}\left\{\frac{1+\eta^2}{\eta^2\left(1+k^2\lambda_{Deff}^2\right)}+3\frac{\lambda_{D,sd}^2}{\lambda_{Deff}^2}\frac{1+\eta^4}{\eta^2\left(1+\eta^2\right)}\right\}^{1/2}, \tag{3.2}$$

the second term on right-hand side is the correction term indicating the dust temperature effects. In the absence of OAM, $l = 0$ which implies that η^2, $\eta^4 \gg 1$ so that the dispersion relation of a plane DA wave is recovered in a permeating dusty plasma (Gong *et al.* 2012*a*). On the other hand, the instability growth rate for twisted DA waves is obtained from the imaginary part of the dielectric constant, as $\omega_i = -D_i(k,\acute{k},\omega)/\partial_{\omega_r}D_r(k,\acute{k},\omega)$;

$$\omega_i = -\sqrt{\frac{\pi}{8}}\frac{\lambda_{Deff}^3}{\lambda_{D,sd}^3}\frac{\omega_r}{\left(1+k^2\lambda_{Deff}^2\right)^{3/2}}\left(\frac{1+\eta^2}{\eta^2}\right)^{1/2}\left[P\left(1-\frac{v_{f0}}{v_{ph}}\right)+Q\right], \tag{3.3}$$

where P and Q are, respectively, given by

$$P = \frac{n_{fi0}}{Z_d^2 n_{sd0}}\left(\frac{T_{sd}}{T_{fi}}\right)^{3/2}\left(\frac{m_{fi}}{m_{sd}}\right)^{1/2}, \tag{3.4}$$

https://doi.org/10.1017/S0022377818000223 Published online by Cambridge University Press

and

$$Q = \frac{n_{se0}}{Z_d^2 n_{sd0}}\left(\frac{T_{sd}}{T_{se}}\right)^{3/2}\left(\frac{m_e}{m_{sd}}\right)^{1/2}\left\{1+\eta\exp\left(-\eta^2\frac{\omega^2}{k^2v_{t,se}^2}\right)\right\} + \frac{n_{si0}}{Z_d^2 n_{sd0}}\left(\frac{T_{sd}}{T_{si}}\right)^{3/2}\left(\frac{m_{si}}{m_{sd}}\right)^{1/2}\left\{1+\eta\exp\left(-\eta^2\frac{\omega^2}{k^2v_{t,si}^2}\right)\right\} + \left\{\exp\left(-\frac{\omega^2}{k^2v_{t,sd}^2}\right)+\eta\exp\left(-\eta^2\frac{\omega^2}{k^2v_{t,sd}^2}\right)\right\} + \eta\frac{n_{fe0}}{Z_d^2 n_{sd0}} \times\left(\frac{T_{sd}}{T_{fe}}\right)^{3/2}\left(\frac{m_e}{m_{sd}}\right)^{1/2}\exp\left(-\eta^2\frac{\omega^2}{k^2v_{t,fe}^2}\right) + \eta\frac{n_{fi0}}{Z_d^2 n_{sd0}}\left(\frac{T_{sd}}{T_{fi}}\right)^{3/2}\left(\frac{m_{fi}}{m_{sd}}\right)^{1/2}\exp\left(-\eta^2\frac{\omega^2}{k^2v_{t,fi}^2}\right). \tag{3.5}$$

Here $m_{se} = m_{fe} = m_e$. In (3.3), the terms in square brackets show that if the streaming speed

$$\frac{v_{f0}}{v_{ph}} > 1 + \frac{Q}{P}, \tag{3.6}$$

then the DA mode becomes unstable. Thus, (3.6) is the threshold condition for instability. In the opposite case, i.e. $v_{f0} < v_{cr}[= \omega_r/k(1+Q/P)]$, the twisted wave is stable showing $\omega_i < 0$. The finite OAM ($l \neq 0$) shows a strong influence on the growth rate (6) via the twist parameter η. Setting $l = 0$, (3.3) can be reduced to the standard solution for a plane wave (Gong *et al.* 2012*a*).

3.2. *High phase speed*

In this case, we assume the thermal speed of the fast moving ions to be much lower than the phase speed of the waves, i.e. $(v_{ph} - v_{f0}) \gg v_{t,fi}$. As a consequence, the arguments are expanded as $C_{z,fe}, C_{z,se}, C_{z,si} \ll 1$, $C_{z,sd}, C_{z,fi} \gg 1$ and $C_{\varphi j} \gg 1$ yielding (Gong *et al.* 2012*a*)

$$D(k,\acute{k},\omega) = 1 + \frac{1}{k^2\lambda_{Deff}'^2} - \frac{\omega_{p,fi}^2}{(\omega - kv_{f0})^2} - \frac{1}{\eta^2}\frac{\omega_{p,fi}^2}{\omega^2} - \frac{\omega_{p,sd}^2}{\omega^2}\left(1+\frac{1}{\eta^2}\right) + 2i\sqrt{\pi}\left[\frac{\omega\omega_{p,se}^2}{k^3v_{t,se}^3}\times\left\{1+\eta\exp\left(-\eta^2\frac{\omega^2}{k^2v_{t,se}^2}\right)\right\} + \frac{\omega\omega_{p,si}^2}{k^3v_{t,si}^3} \times\left\{1+\eta\exp\left(-\eta^2\frac{\omega^2}{k^2v_{t,si}^2}\right)\right\} + \frac{\omega\omega_{p,sd}^2}{k^3v_{t,sd}^3}\left\{\exp\left(-\frac{\omega^2}{k^2v_{t,sd}^2}\right) + \eta\exp\left(-\eta^2\frac{\omega^2}{k^2v_{t,sd}^2}\right)\right\} + (\omega - kv_{f0}) \times\left\{\frac{\omega_{p,fe}^2}{k^3v_{t,fe}^3} + \frac{\omega_{p,fi}^2}{k^3v_{t,fi}^3}\exp\left(-\frac{(\omega-kv_{f0})^2}{k^2v_{t,fi}^2}\right)\right\} + \frac{\omega\omega_{p,fe}^2}{k^3v_{t,fe}^3}\eta\exp\left(-\eta^2\frac{\omega^2}{k^2v_{t,fe}^2}\right) + \frac{\omega\omega_{p,fi}^2}{k^3v_{t,fi}^3}\eta\exp\left(-\eta^2\frac{\omega^2}{k^2v_{t,fi}^2}\right)\right]. \tag{3.7}$$

https://doi.org/10.1017/S0022377818000223 Published online by Cambridge University Press

Here, the effective Debye length is defined as $\lambda'^{-2}_{Deff}[=\lambda^{-2}_{D,se}+\lambda^{-2}_{D,si}+\lambda^{-2}_{D,fe}]$. In this case, the frequency of the twisted DA wave becomes

$$\omega_r = \frac{k\lambda'_{Deff}\omega_{p,sd}}{\left(1+k^2\lambda'^2_{Deff}\right)^{1/2}}\left[\frac{\omega^2_{p,fi}}{\omega^2_{p,sd}}\left\{\frac{1}{\left(1-v_{f0}/v_{ph}\right)^2}+\frac{1}{\eta^2}\right\}+\left(1+\frac{1}{\eta^2}\right)\right]^{1/2}. \tag{3.8}$$

The corresponding instability growth rate of the twisted DA wave gives

$$\omega_i = -\sqrt{\frac{\pi}{8}}\frac{\lambda'^3_{Deff}}{\lambda^3_{D,sd}}\frac{\omega_r}{\left(1+k^2\lambda'^2_{Deff}\right)^{3/2}}\left\{\frac{n_{fi0}}{Z^2_d n_{sd0}}\frac{m_{sd}}{m_{fi}}\left(\frac{1}{\left(1-v_{f0}/v_{ph}\right)^2}+\frac{1}{\eta^2}\right)+\left(1+\frac{1}{\eta^2}\right)\right\}^{1/2}\left[P'\left(1-\frac{v_{f0}}{v_{ph}}\right)+Q'\right], \tag{3.9}$$

where

$$P' = \frac{n_{fe0}}{Z^2_d n_{sd0}}\left(\frac{T_{sd}}{T_{fe}}\right)^{3/2}\left(\frac{m_e}{m_{sd}}\right)^{1/2}+\frac{n_{fi0}}{Z^2_d n_{sd0}}\left(\frac{T_{sd}}{T_{fi}}\right)^{3/2}\times\left(\frac{m_{fi}}{m_{sd}}\right)^{1/2}\exp\left(-\frac{(\omega-kv_{f0})^2}{k^2v^2_{t,fi}}\right), \tag{3.10}$$

while $Q'=Q$. Equation 3.9 satisfies the following instability condition

$$\frac{v_{f0}}{v_{ph}} > 1+\frac{Q'}{P'}, \tag{3.11}$$

which is the onset of the instability. For neglecting the OAM effect, the parameter η simply tends to infinity and a straight propagating DA plane wave is obtained in a permeating dusty plasma (Gong *et al.* 2012*a*). The expressions clearly indicate that instability threshold in this case is different from the previous case and will also be elaborated numerically.

4. Twisted dust-ion-acoustic wave and instability

To investigate the twisted dust-ion-acoustic (DIA) wave and instability on the ion time scale, *viz.*, $v_{t,si} \ll v_{ph} \ll v_{t,se}, v_{t,fe}, v_{t,fi}$, we assume that streaming electrons and ions are penetrating through a dusty plasma containing the inertialess electrons, dynamical ions and static dust grains in the background. For small and large argument expansions, $C_{zfe}, C_{zfi}, C_{zse} \ll 1$ and $C_{zsi}, C_{\varphi j} \gg 1$ in (2.3), we arrive at the following dispersion relation

$$\omega_r = k\lambda''_{Deff}\omega_{p,si}\left\{\frac{1+\eta^2}{\eta^2\left(1+k^2\lambda''^2_{Deff}\right)}+3\frac{T_{si}}{T_{se}}\left(1-Z_d\delta-\frac{n_{fe0}}{n_{si0}}+\frac{n_{fi0}}{n_{si0}}+\frac{n_{fe0}}{n_{si0}}\frac{T_{se}}{T_{fe}}+\frac{n_{fi0}}{n_{si0}}\frac{T_{se}}{T_{fi}}\right)\frac{1+\eta^4}{\eta^2\left(1+\eta^2\right)}\right\}^{1/2}, \tag{4.1}$$

where $\delta = n_{sd0}/n_{si0}$ and $\lambda''_{Deff} = (\lambda^{-2}_{D,se}+\lambda^{-2}_{D,fe}+\lambda^{-2}_{D,fi})^{-1/2}$. For an electron–ion plasma, we assume a dust density $n_{sd0}=0,$, as a result, standard ion-acoustic waves propagate in

https://doi.org/10.1017/S0022377818000223 Published online by Cambridge University Press

a permeating plasma. Furthermore, if there is only a slow moving plasma i.e. $n_{fe0} = n_{fi0} = 0$, the dispersion relation of the twisted DIA waves retrieves

$$\omega_r = kC_{dia}\left\{\frac{1+\eta^2}{\eta^2(1+k^2\lambda_{Dse}^2)} + \frac{3T_{si}}{T_{se}}\frac{1+\eta^4}{\eta^2(1+\eta^2)}(1-Z_{d0}\delta)\right\}^{1/2}, \tag{4.2}$$

which exactly agrees with Ali *et al.* (2016). The DIA speed can be expressed, as

$$C_{dia} = \omega_{p,si}\lambda_{D,se} = \frac{(T_{se}/m_{si})^{1/2}}{(1-Z_{d0}\delta)^{1/2}}. \tag{4.3}$$

Similarly, the imaginary part of the DIA waves is given by

$$\begin{aligned}\omega_i \;=\; & -\sqrt{\frac{\pi}{8}}\frac{\left((1+\eta^2)/\eta^2\right)^{1/2}}{\left\{\frac{T_{si}}{T_{se}}\left(1-Z_d\delta-\frac{n_{fe0}}{n_{si0}}+\frac{n_{fi0}}{n_{si0}}+\frac{n_{fe0}}{n_{si0}}\frac{T_{se}}{T_{fe}}+\frac{n_{fi0}}{n_{si0}}\frac{T_{se}}{T_{fi}}\right)\right\}^{3/2}} \\ & \times\frac{\omega_r}{\left(1+k^2\lambda_{Deff}''^2\right)^{3/2}}\left[P''\left(1-\frac{v_{f0}}{v_{ph}}\right)+Q''\right],\end{aligned} \tag{4.4}$$

where

$$P'' = \frac{n_{fi0}}{n_{si0}}\left(\frac{T_{si}}{T_{fi}}\right)^{3/2}\left(\frac{m_{fi}}{m_{si}}\right)^{1/2}, \tag{4.5}$$

and

$$\begin{aligned}Q'' \;=\; & \left(1-Z_d\delta-\frac{n_{fe0}}{n_{si0}}+\frac{n_{fi0}}{n_{si0}}\right)\left(\frac{T_{si}}{T_{se}}\right)^{3/2}\left(\frac{m_e}{m_{si}}\right)^{1/2} \\ & \times\left\{1+\eta\exp\left(-\eta^2\frac{\omega^2}{k^2v_{t,se}^2}\right)\right\} \\ & +\left\{\exp\left(-\frac{\omega^2}{k^2v_{t,si}^2}\right)+\eta\exp\left(-\eta^2\frac{\omega^2}{k^2v_{t,si}^2}\right)\right\} \\ & +\eta\frac{n_{fe0}}{n_{si0}}\left(\frac{T_{si}}{T_{fe}}\right)^{3/2}\left(\frac{m_e}{m_{si}}\right)^{1/2}\exp\left(-\eta^2\frac{\omega^2}{k^2v_{t,fe}^2}\right) \\ & +\eta\frac{n_{fi0}}{n_{si0}}\left(\frac{T_{si}}{T_{fi}}\right)^{3/2}\left(\frac{m_{fi}}{m_{si}}\right)^{1/2}\exp\left(-\eta^2\frac{\omega^2}{k^2v_{t,fi}^2}\right).\end{aligned} \tag{4.6}$$

For $n_{sd0} = 0$, the growth rate of the standard ion-acoustic waves is obtained in a permeating plasma. Furthermore, if $n_{fe0} = n_{fi0} = 0$, and $v_{f0} = 0$ but $n_{sd0} \neq 0$ this gives an expression for the Landau damping of the twisted DIA waves in a multi-component dusty plasma (Ali *et al.* 2016).

Now, from (4.4), the necessary condition for instability turns out to be

$$\frac{v_{f0}}{v_{ph}} > 1 + \frac{Q''}{P''}. \tag{4.7}$$

The influence of finite OAM states on the instability growth rate is dictated by the twist parameter η and will be explained in the following section.

https://doi.org/10.1017/S0022377818000223 Published online by Cambridge University Press

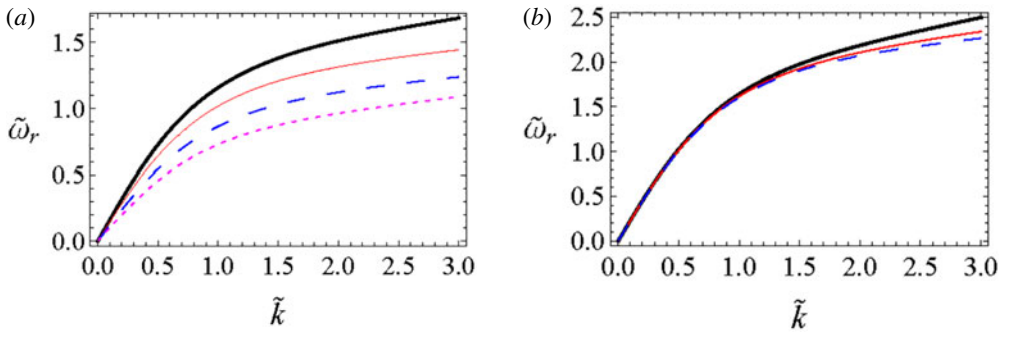


FIGURE 1. Case A: the normalized twisted DA frequency ($\tilde{\omega}_r = \omega_r/\omega_{p,sd}$) is plotted against the normalized wavenumber ($\tilde{k} = k\lambda_{Deff}$) for varying (*a*) the twist parameter $\eta = 0.8$ (thick solid black curve), $\eta = 1$ (thin solid red curve), $\eta = 1.5$ (large dashed blue curve), $\eta = 50$ (small dashed pink curve) with fixed $Z_d = 800$ and (*b*) the dust charging state $Z_d = 600$ (thick solid black curve), 800 (thin solid red curve), 1000 (large dashed blue curve) with fixed $\eta = 0.5$.

5. Results and discussion

In this section, we present a parametric study of the effects of the different plasma parameters, namely, the twist parameter η owing to the helical phase structure, the dust charge number Z_d and the streaming velocities of the fast moving plasma species, on the frequency and growth rate of twisted DA and DIA waves in a multi-component permeating dusty plasma. From an application point of view, we have applied our model to the streaming solar wind plasma penetrating into a cometary dusty plasma and have chosen the physical parameters from a cometary plasma environment (Angelo 1998); e.g. $n_{si0} = 10$ cm^{-3}, $n_{d0} = 0.00001$ cm^{-3}, $Z_d = 800$, $m_{sd} = 1.13 \times 10^{-17}$ g, $T_{se} = 1.16 \times 10^5$ K, $T_{si} = 2.32 \times 10^4$ K and $T_{sd} = 1.16 \times 10^2$ K, with a mean radius of the dust grains of $a_r = 3 \times 10^{-6}$ cm. We also made use of numerical values (Vranjes 2011) for the electrons and ions from solar wind plasma, e.g. $T_{fe} = T_{fi} = 1.5 \times 10^5$ K, $n_{fe0} = n_{fi0} = 5$ cm^{-3}, and $m_{fi} = 1.67 \times 10^{-24}$ g with a solar wind speed $v_{fe0} = v_{fi0} = v_{f0} = 5 \times 10^7$ cm s^{-1}.

In figure 1, we examine the influence of (*a*) finite OAM states (l) via the twist parameter $\eta (= k/lq_\varphi)$ at $Z_d = 800$ and (*b*) the dust charge state Z_d at fixed $\eta = 0.5$ on the dispersion curves of twisted DA waves in the low phase speed limit, $v_{ph} - v_{f0} \ll v_{t,fi}$. Due to the presence of the twist parameter, the wave frequency of the twisted DA waves is increased as compared to the plane propagating DA waves. Figure 1(*b*) shows how the dust charge state decreases the wave frequency of the DA waves. Figure 2 exhibits the contours of the normalized twisted DA wave frequency $\tilde{\omega}_r$ in the limit of high phase speed, *viz.*, $v_{ph} - v_{f0} \gg v_{t,fi}$, against the normalized wavenumber $\tilde{k}$ and twist parameter η at $Z_d = 800$. The contours indicate that the wave frequency of the DA waves clearly reduces as we move from the lower values of η towards higher values of η (approaching to planner wave solution). The enhancement of parameter η corresponds to a lower value of OAM state l. Thus, whether the phase speed limit is taken as low or high, the twisted wave appears as a slow wave in comparison to the planner wave solution.

Figure 3 displays the three-dimensional variation of the damping and growth rates (case A of § 3) as a function of normalized wavenumber and normalized streaming velocity for two different values of the twist parameter, *viz.*, $\eta = 0.5$ (figure 3*a*,*b*), and

https://doi.org/10.1017/S0022377818000223 Published online by Cambridge University Press

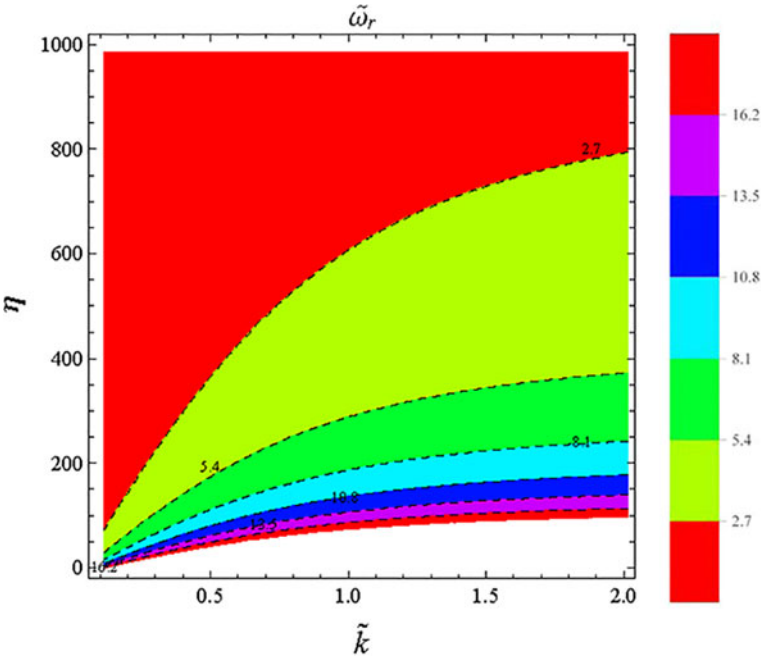


FIGURE 2. Case B: the contours of the normalized twisted DA wave frequency ($\tilde{\omega}_r = \omega_r/\omega_{p,sd}$) are shown against the normalized wavenumber ($\tilde{k} = k\lambda'_{Deff}$) and twist parameter η at fixed $Z_d = 800$.

$\eta = 1.2$ (figure 3(*c*,*d*). It is found that the instability threshold has strong dependence on the twist parameter, giving rise to $v_{cr} = (1 + Q/P)v_{ph} \approx 53C_{da}$ for $\eta = 0.5$, assuming that the azimuthal wavenumber is large compared to the plane wavenumber $\tilde{k} = 2.0$. For values below this critical value, $v_{f0} < 53C_{da}$, the twisted DA wave remains damped while above this limit, the behaviour of the twisted wave changes and it starts to grow. Moreover, in a situation where the azimuthal wavenumber becomes smaller than the plane wavenumber (see figure 3(*c*,*d*) by taking the twist parameter as $\eta = 1.2$, the instability threshold then reduces to $v_{cr} \approx 45C_{da}$ and consequently the magnitude of the growth rate reduces with the enhancement of η, implying that as we move towards the planner wave solution, the growth rate decreases correspondingly. Hence, the twisted waves are more unstable than the planner waves under certain plasma parameters. In figure 4, the contours of the damping and growth rates associated with DA waves are displayed as a function of normalized wavenumber and twist parameter for the high phase speed limit $v_{ph} - v_{f0} \gg v_{t,fi}$. It is observed that for wavelengths greater than or equal to the unity, $\tilde{k} \leqslant 1$, the DA waves become Landau damped while for smaller wavelengths, $\tilde{k} > 1$, the growth rates of the DA wave appear in the permeating dusty plasma. Hence, due to the presence of a free energy source, the DA planner waves grow as compared to twisted waves.

To examine the impact of the twist parameter and dust concentration on the DIA waves in the multi-component permeating dusty plasma, the curves of DIA wave frequency ($\tilde{\omega}_r = \omega_r/\omega_{psi}$) are represented as a function of the normalized wavenumber ($\tilde{k} = k\lambda''_{Deff}$) for different values of the twist parameter $\eta(= 0.8, 1, 1.2, 50)$ as shown in figure 5. A reduction in the twisted wave frequency occurs (see figure 5*a*) when

https://doi.org/10.1017/S0022377818000223 Published online by Cambridge University Press

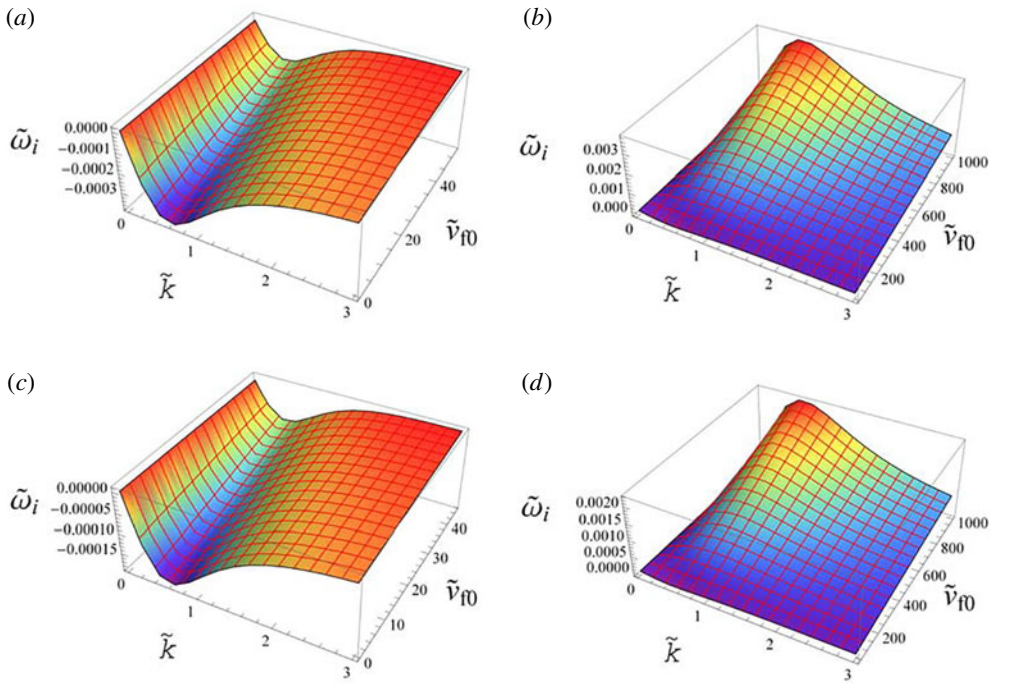


FIGURE 3. Case A: three-dimensional plots showing the damping rates at (*a*) $\eta = 0.5$, (*c*) $\eta = 1.2$ and instability growth rates of twisted DA waves at (*b*) $\eta = 0.5$ and (*d*) $\eta = 1.2$ against the normalized wavenumber $\tilde{k}$ and streaming velocity of the fast moving species ($\tilde{v}_{f0}$). Other parameters are the same as given in § 5.

we move to the plane propagating DIA waves while the dust concentration also modifies the twisted wave frequencies (see figure 5*b*). To investigate numerically the Landau damping/growth rates involving the twisted DIA waves as a function of the normalized wavenumber and normalized streaming speed, three-dimensional plots are shown in figure 6. It may be noticed that the twisted DIA waves can be excited above the critical value, *viz.*, $v_{cr} \approx 2.45 C_{dia}$ when taking into account the values of the twist parameter $\eta = 0.5$ and longitudinal wavenumber $\tilde{k} = 1.5$. See that for $v_{f0} < v_{cr}$, the twisted wave is damped while in the opposite limit, $v_{f0} > v_{cr}$, the instability growth rate appears and increases with the enhancement of the streaming speed. Furthermore, when the longitudinal wavenumber dominates the azimuthal wavenumber, which implies that $\eta = 1.2$, the magnitude of the expression $[v_{cr} = (1 + Q''/P'')v_{ph} \approx 1.48 C_{dia}]$ reduces. The plots in figure 6(*c*,*d*) indicate the damping and growth rates corresponding to $v_{f0} < v_{cr}$ and $v_{f0} > v_{cr}$, respectively. The enhancement of the twist parameter leads to the reduction of the damping and growth rates, showing that planner waves are less unstable as compared to twisted waves.

6. Summary

To summarize, we have considered a permeating dusty plasma environment and investigate the properties of the twisted DA and DIA waves and instabilities using the kinetic description. The plasma model can be solved by taking into account the LG profiles for the perturbed distribution function and wave potential, deriving a

https://doi.org/10.1017/S0022377818000223 Published online by Cambridge University Press

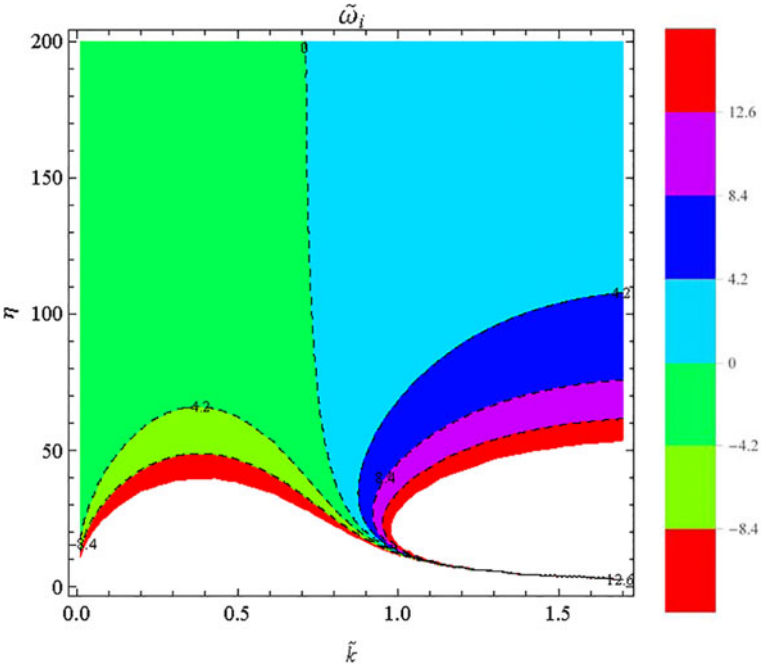


FIGURE 4. Case B: contours of the twisted DA waves ($\tilde{\omega}_i$) as a function of normalized wavenumber $\tilde{k}$ and twist parameter η at $v_{f0} = 1.8 \times 10^6$ cm s^{-1}.

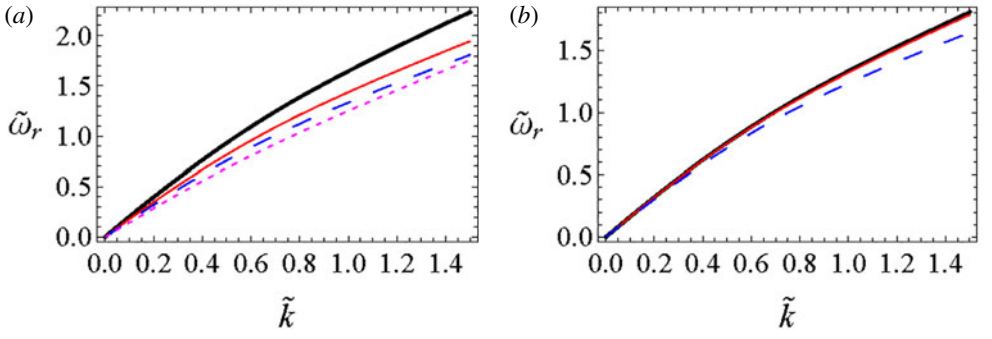


FIGURE 5. The normalized twisted DIA frequency ($\tilde{\omega}_r = \omega_r/\omega_{p,si}$) is depicted against the normalized wavenumber ($\tilde{k} = k\lambda''_{Deff}$) for varying (*a*) the twist parameter $\eta = 0.8$ (thick solid black curve), $\eta = 1$ (thin solid red curve), $\eta = 1.2$ (dashed blue curve), $\eta = 50$ (small dashed pink curve) at $Z_d = 800$ and (*b*) dust concentration $\delta = 0, 5 \times 10^{-5}, 1 \times 10^{-4}$ at $\eta = 1.2$.

generalized dielectric constant in the limit of paraxial approximation. The dispersion relations are analysed to show kinetic instabilities by identifying the threshold conditions for the damping/growth rates. A general criterion for instability of DIA waves is discussed while for the DA waves, two specific limiting cases are considered, when (A) the thermal velocity of the fast moving plasma is much larger than the phase speed of the waves and (B) the thermal velocity of the fast moving plasma is much smaller than the phase speed of the waves. It is shown that the frequency

https://doi.org/10.1017/S0022377818000223 Published online by Cambridge University Press

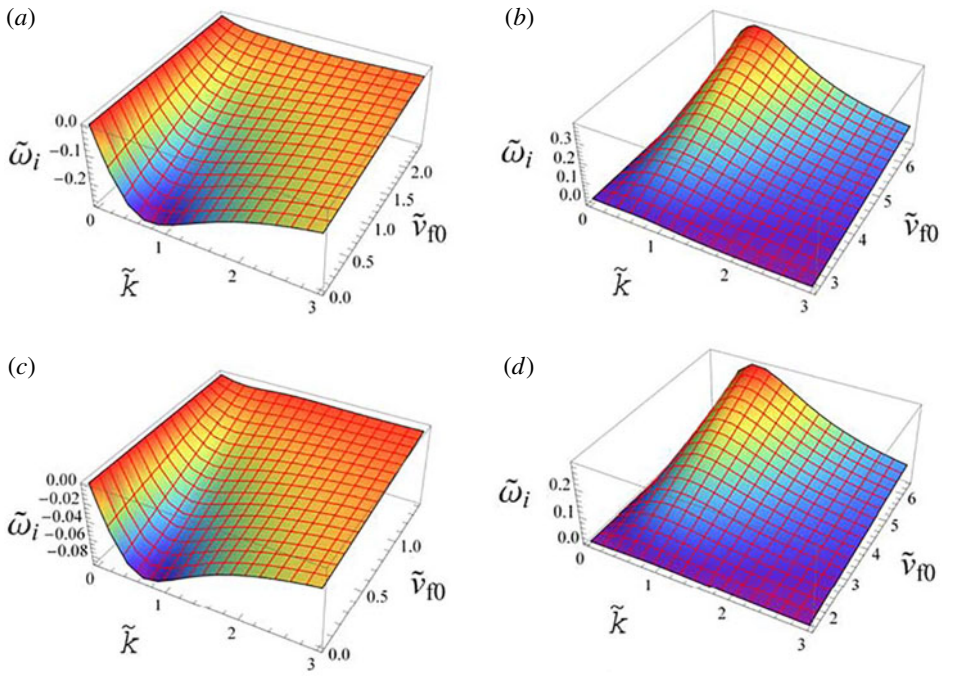


FIGURE 6. Three-dimensional plots showing the damping rates at (*a*) $\eta = 0.5$, (*c*) $\eta = 1.2$ and instability growth rates of the twisted DA waves at (*b*) $\eta = 0.5$ and (*d*) $\eta = 1.2$ against the normalized wavenumber $\tilde{k}(= k\lambda''_{Deff})$ and streaming velocity of the fast moving species $\tilde{v}_{f0}(= v_{f0}/C_{dia})$. Other parameters are the same as given in § 5.

and growth rates of the twisted waves in multi-component permeating plasmas are significantly affected by the plasma parameters, such as the twist parameter, the streaming velocity and the dust concentration. The present analysis is important in plasma environments where solar/stellar winds penetrate into the interstellar plasma and cometary tails.

REFERENCES

ALI, S., BUKHARI, S. & MENDONCA, J. T. 2016 Twisted Landau damping rates in multi-component dusty plasmas. *Phys. Plasmas* **23**, 033703.

ANGELO, N. D. 1998 Current-driven electrostatic dust-cyclotron instability in a collisional plasma. *Planet. Space Sci.* **46**, 1671.

ARSHAD, K., LAZAR, M., MAHMOOD, S., REHMAN, A. & POEDTS, S. 2017 Kinetic study of electrostatic twisted waves instability in nonthermal dusty plasmas. *Phys. Plasmas* **24**, 033701.

BALSIGER, H., ALTWEGG, K., BHLER, F., GEISS, J., GHIELMETTI, A. G., GOLDSTEIN, B. E., GOLDSTEIN, R., HUNTRESS, W. T., LAZARUS, A. J., MEIER, A. *et al.* 1986 Ion composition and dynamics at comet Halley. *Nature* **321**, 330.

BUKHARI, S., ALI, S., RAFIQUE, M. & MENDONCA, J. T. 2017 Twisted electrostatic waves in a self-gravitating dusty plasma. *Contrib. Plasma Phys.* **57**, 404.

FESTAU, M. C., KELLER, H. U. & WEAVER, H. A. 2004 A Brief conceptual cistory of Cometary Science. In *Comets II*, University of Arizona Press.

GONG, J., LIU, Z. & DU, J. 2012*a* Dust-acoustic waves and stability in the permeating dusty plasma. I. Maxwellian distribution. *Phys. Plasmas* **19**, 043704.

https://doi.org/10.1017/S0022377818000223 Published online by Cambridge University Press

GONG, J., LIU, Z. & DU, J. 2012*b* Dust-acoustic waves and stability in the permeating dusty plasma. II. Power-law distributions. *Phys. Plasmas* **19**, 083706.

GRARD, R., PEDERSEN, A., TROTIGNON, J. G., BEGHIN, C., MOGILEVSKY, M., MIKHAILOV, Y., MOLCHANOV, O. & FORMISANO, V. 1986 *Nature* **321**, 290.

GREWING, M., PRADERIE, F. & REINHARD, R. 1988 *Exploration of Halley's Comet*. Springer.

KHAN, S. A., REHMAN, A. & MENDONCA, J. T. 2014 Kinetic study of ion-acoustic plasma vortices. *Phys. Plasmas* **21**, 092109.

KLIMOV, S., SAVIN, S., ALEKSEVICH, Y., AVANESOVA, G., BALEBANOV, V., BALIKHIN, M., GALEEV, A., GRIBOV, B., NOZDRACHEV, M., SMIRNOV, V. *et al.* 1986 Extremely-low-frequency plasma waves in the environment of comet Halley. *Nature* **321**, 292.

KLUMOV, B. A., VLADIMIROV, S. V. & MORFILL, G. E. 2005 Features of dusty structures in the upper Earth's atmosphere. *JEPT Lett.* **82**, 632.

KLUMOV, B. A., VLADIMIROV, S. V. & MORFILL, G. E. 2007 On the role of dust in the cometary plasma. *JEPT Lett.* **85**, 478.

LUNDIN, R. & MARKLUND, G. 1995 Plasma vortex structures and the evolution of the solar system the legacy of Hannes Alfvén. *Phys. Scr.* **T60**, 198.

MENDIS, D. A. 1988 A postencounter view of Comets. *Annu. Rev. Astron. Astrophys.* **26**, 11.

MENDIS, D. A. & HORANYI, M. 2013 Dusty plasma effects in Comet: expectations for ROSETTA. *Rev. Geophys.* **51**, 53.

MENDONCA, J. T. 2012 Kinetic description of electron plasma waves with orbital angular momentum. *Phys. Plasmas* **19**, 112113.

MENDONCA, J. T., THIDE, B. & THEN, H. 2009 Stimulated Raman and Brillouin backscattering of collimated beams carrying orbital ongular oomentum. *Phys. Rev. Lett.* **102**, 185005.

SHAHZAD, K. & ALI, S. 2014 Finite orbital angular momentum states and Laguerre–Gaussian potential in two-temperature electron plasmas. *Astrophys. Space Sci.* **3**, 353.

SHUKLA, P. K. 2012 Twisted dust acoustic waves in dusty plasmas. *Phys. Plasmas* **19**, 083704.

SIBECK, D. G. 1990 A model for the transient magnetospheric response to sudden solar wind dynamic pressure variations. *J. Geophys. Res.* **95**, 3755.

STENZEL, R. L. 2016 Whistler waves with angular momentum in space and laboratory plasmas and their counterparts in free space. *Adv. Phys. X* **1**, 687.

VRANJES, J. 2011 Current-less solar wind driven dust acoustic instability in cometary plasma. *Phys. Plasmas* **18**, 084501.

VRANJES, J. & POEDTS, S. 2014 Ion acoustic mode in permeating plasmas. *J. Phys. Conf. Ser.* **511**, 012010.

WURZ, P., RUBIN, M., ALTWEGG, K., BALSIGER, H., BERTHELIER, J. J., BIELER, A., CALMONTE, U., KEYSER, J. D., FIETHE, B., FUSELIER, S. A. *et al.* 2015 Solar wind sputtering of dust on the surface of 67P/Churyumov-Gerasimenko. *Astron. Astrophys.* **583**, 22.

YAROSHENKO, V., LUHR, H. & MILOCH, W. J. 2014 Dust charging in the Enceladus torus. *J. Geophys. Res. Space Phys.* **119**, 221.

YAROSHENKO, V., MILOCH, W. J. & LÜHR, H. 2015 Particle-in-cell simulation of spacecraft/plasma interactions in the vicinity of Enceladus. *Icarus* **257**, 1.

YAROSHENKO, V., MILOCH, W. J., VLADIMIROV, S., THOMAS, H. M. & MORFILL, G. E. 2011 Modeling of Cassini's charging at Saturn orbit insertion flyby. *J. Geophys. Res.* **116**, 12218.

YAROSHENKO, V., RATYNSKAIA, S., OLSON, J., BRENNING, N., WAHLUND, J. E., MOROOKA, M., KURTH, W. S., GURNETT, D. A. & MORFILL, G. E. 2009 Characteristics of charged dust inferred from the Cassini RPWS measurements in the vicinity of Enceladus. *Planet. Space Sci.* **57**, 1807.

https://doi.org/10.1017/S0022377818000223 Published online by Cambridge University Press